JOURNAL OF GEOPHYSICAL RESEARCH, VOL. 106, NO. D11, PAGES 11,849–11,858, JUNE 16, 2001

Observations of high-frequency temporal gravity wave spectra in the middle upper stratosphere

A. T. Russell and R. J. Sica

Department of Physics and Astronomy, The University of Western Ontario, London, Ontario, Canada

Abstract. There is a paucity of high-frequency temporal gravity wave spectra in the middle upper stratosphere (30-40 km) as most instruments that are capable of accessing this region do not have the capability to make measurements for any extended period of time. The spectral analysis of density fluctuations obtained with the Purple Crow Rayleigh scatter lidar has shown that middle upper stratospheric temporal spectra follow the expected -1.5 to -2.0 power law relationship for frequencies less than 1 x 10^{-3} s^{-1}. At frequencies greater than 1 x 10^{-3} s^{-1}, the shape of the temporal spectrum is much more variable, with strong quasi-monochromatic features appearing intermittently on certain nights. These higher-frequency features have been attributed to nonlinear wave interactions and suggest that estimates of gravity wave activity in the middle upper stratosphere may be larger and much more variable than previously assumed. This variability also suggests that middle upper stratospheric energy dissipation and eddy diffusion values may be much larger and more variable than previously assumed. Current parameterizations of subgrid dynamical processes in general circulation models that resolve this region may need to be reexamined in this light.

1. Introduction

The importance of gravity wave motions in maintaining the structure and large-scale circulation of the middle atmosphere has spurred many observational studies on mesoscale motions throughout the atmosphere. Some of these observational studies have focused on the characteristics of quasi-monochromatic gravity wave motions that tend to dominate the gravity wave field [e.g., *Moreels and Hearse*, 1977; *Cot and Barat*, 1986; *Gardner and Volez*, 1987; *Manson*, 1990; *Beatty et al.*, 1992], providing valuable information on the amplitudes, phase speeds, periods, and wavelengths of such waves. Other observational studies have concentrated on long-term gravity wave effects and climatologies, allowing one to characterize these gravity wave effects in terms of their variances and spectra [e.g., *Hirota*, 1984; *Vincent and Fritts*, 1987; *Gardner et al.*, 1989a; *Tsuda et al.*, 1994; *Whiteway and Carswell*, 1995; *Allen and Vincent*, 1995; *Bacmeister et al.*, 1996; *Collins et al.*, 1996]. The statistical characterization of these integrated, long term effects is very important to our understanding of the lower and middle atmosphere, especially when one attempts to parameterize these effects in global circulation models [*Hamilton*, 1997].

One of the most important complications when one tries to interpret the temporal spectra of propagating gravity waves is the fact that the observed frequencies of the gravity waves have been Doppler-shifted by the mean flow. Several authors [i.e., *Scheffler and Liu*, 1986; *Fritts and VanZandt*, 1987; *Gardner et al.*, 1993] have attempted to model these Doppler-shifting effects on temporal gravity wave spectra and have found that significant amounts of energy can be Doppler-shifted past the buoyancy frequency, resulting in shallower spectral slopes at higher frequencies. This prediction is in general agreement with most of the observed frequency spectra in the troposphere, lower stratosphere, upper mesosphere, and lower thermosphere.

Another characteristic of some temporal spectra is an increase in energy at frequencies just below the observed local buoyancy frequency. This increase in energy is usually attributed to the constructive interference of higher-frequency gravity waves [*Desaubies*, 1975; *VanZandt*, 1985] and has been observed in the vertical velocity spectra of the troposphere, lower stratosphere, and lower thermosphere [*Tolstoy and Montes*, 1971; *Rottger*, 1981; *Ecklund et al.*, 1985, *Meek et al.*, 1985], as well as the vertical displacement spectra of the oceans [*Voorhis*, 1968; *Gould*, 1971; *Briscoe*, 1975; *Cairns*, 1975].

Most of the spectral studies that have been mentioned so far have involved radiosondes, aircraft, sodium lidar, or MF/mesosphere-stratosphere-troposphere (MST) radar observations of neutral atmospheric winds, which have resulted in a paucity of high-resolution frequency spectra in the 25 to 60 km altitude region. The Purple Crow Rayleigh scatter lidar (PCRSL), with its large power-aperture product, has the capability to make continuous, high-resolution, measurements in the upper stratosphere and lower mesosphere, filling in this "gap" region. High-resolution middle upper stratospheric frequency spectra from the PCRSL database will be presented, with several of these spectra exhibiting features at frequencies greater than 1.67 x 10^{-3} s^{-1} (1/(10 min)).

2. Methodology

The Purple Crow Rayleigh scatter lidar (PCRSL) is a large power-aperture product Rayleigh scatter lidar that has been designed to measure temperatures and density fluctuations in the upper stratosphere and lower mesosphere at high spatial-temporal resolution. This large power-aperture product in the PCRSL has been obtained by combining a frequency-doubled 12 W Nd:YAG

Paper number 2000JD900644.
0148-0227/01/2000JD900644$09.00

laser with a 2.65 m diameter liquid mercury telescope. A thorough description of the PCRSL system has been given by *Sica et al.* [1995].

The signal-processing routines used in this study are based on the work of *Gardner et al.* [1989b] and *Sica and Russell* [1999]. The raw photocount profiles obtained with the PCRSL have a range resolution of 24 m and an integration period of 1 min. These raw photocount profiles are corrected for any nonlinearities in the PCRSL photon counting system as the accurate retrieval of the raw photocount profiles is important in determining the relative density fluctuations used in this study. The corrected photocount profiles are then coadded to a resolution of 48 m in the vertical and 1 min in time. These corrected and coadded photocount profiles are then converted into relative density profiles by multiplying by the square of the range.

The relative density fluctuation field is then formed by removing an unperturbed basic state estimate from each relative density profile (this unperturbed basic state estimate is formed by fitting a third-order polynomial to the average relative density profile for that night). The resulting relative density fluctuation field is then filtered spatially with a 1008 m cutoff Kaiser-Bessel filter, which reduces the variance of the relative density fluctuation field by a factor of 16.2. Individual time series within this fluctuation field then have their mean removed. The resulting time series are spectrally analyzed using the covariance method of autoregressive power spectral density (PSD) estimation [*Marple*, 1987]. Model orders for this method of spectral estimation are selected by a signal/noise floor eigenvalue criterion that is similar to that described by *Sica and Russell* [1999]. These autoregressive PSD estimates are consistent with the correlogram method of PSD estimation, but only the autoregressive PSD results will be presented in this study as the correlogram PSDs have a lower spectral resolution and exhibit a lower frequency rollover that is endemic to all correlogram PSD estimators.

After the removal of the photon noise floors, the individual PSD estimates are scaled by [*Gardner et al.*, 1989a]

$$\zeta(z) = \frac{1}{2}\,\rho(z)\left[\frac{g(z)}{2\pi N_b(z)}\right]^2 \qquad (1)$$

and averaged together to form the mean horizontal kinetic energy spectral density (KESD) estimate. The $g(z)$, $\rho(z)$, and $N_b(z)$ terms in (1) are the gravitational field strength and the measured buoyancy frequency and density profiles, respectively. The mean horizontal kinetic energy spectral content (KESC) estimates can also estimated by weighting the individual KESD estimates by the appropriate frequencies, that is, $KESC(f) = f\,KESD(f)$.

Since intrinsic gravity wave frequencies cannot exceed the measured buoyancy frequency, it will be assumed that any energy observed beyond the measured buoyancy frequency is due to Doppler-shifting effects. This amount of energy will be quantified by integrating the KESD estimates from the measured buoyancy frequency to the Nyquist frequency using a simple trapezoidal integration scheme. The amount of energy present in the noise floors can be estimated in a similar manner. It should be noted that the photon noise floor energies will increase with height because the measurement signal-to-noise ratio decreases with height.

3. Results

Three nights of measurements were selected for this study: August 30, 1994, August 22, 1995, and October 13, 1995. All three of these nights have at least 6 hours of continuous measurements. The temporal spectrum on the night of August 22, 1995 is a

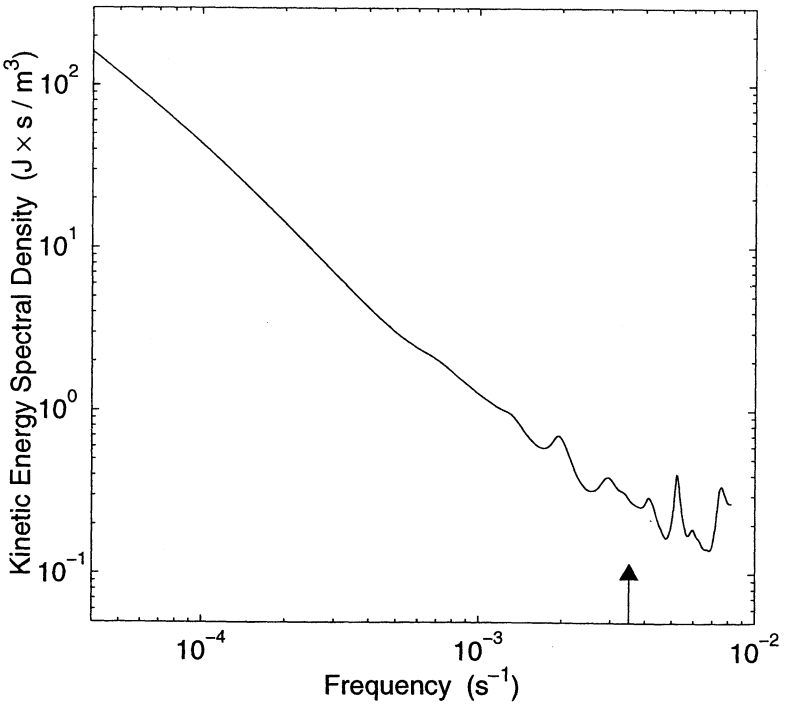

Figure 1. Temporal kinetic energy (KE) spectrum on the night of August 22, 1995, averaged over the altitude interval 35.0 - 41.0 km. The photon noise floor has a mean value of 0.41 mJ s m^{-3} and has been removed from the spectrum. The arrow on the frequency axis indicates the average value of the measured buoyancy frequency for the altitude range under consideration (3.51 x 10^{-3} s^{-1}).

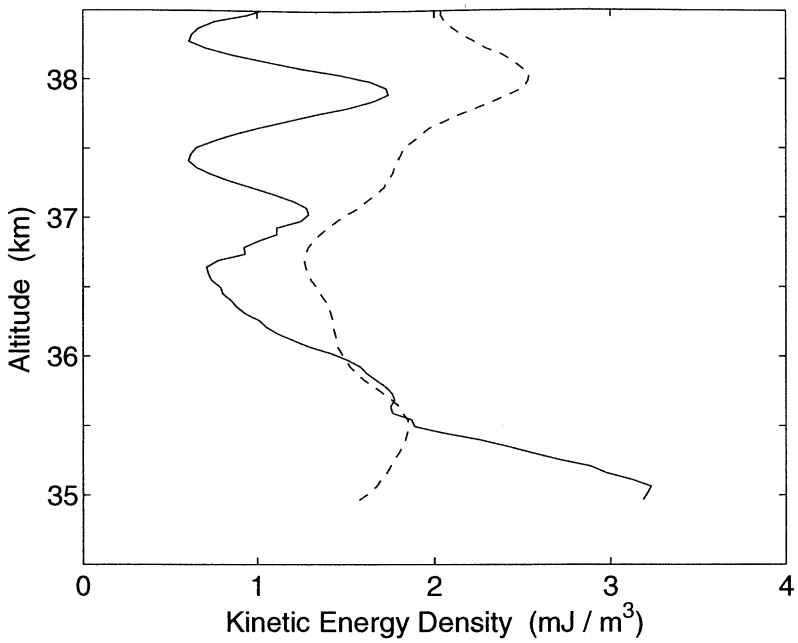

Figure 2. Estimated energy at frequencies greater than the buoyancy frequency on the night of August 22, 1995. The solid line represents the amount of energy past the buoyancy frequency in the KE spectra with the noise floor removed. The dashed line represents the amount of energy past the buoyancy frequency due to photon noise.

classic example of a "textbook" frequency spectrum and illustrates the reliability of the methodology used in this study. The spectra obtained on the nights of August 30, 1994 and October 13, 1995 are more "exotic", with higher- frequency features being present in both spectra. Excesses of energy occurring at frequencies just below the measured buoyancy frequency and at frequencies greater than the measured buoyancy frequency were also observed in the August 30 and October 13 spectra.

3.1. August 22, 1995

Measurements on this night commenced at 0238 UT (2238 LT) and ended at 0843 UT. The mean temporal KESD estimate over the altitude interval 35.0 - 41.0 km is shown in Figure 1, and as already noted, is a classic example of the "typical" frequency spectrum as the spectrum has a slope of -1.54 ± 0.01 in the frequency range 4.65×10^{-5} s^{-1} to 1.00×10^{-3} s^{-1} and exhibits some minor Doppler-shifting effects. These Doppler-shifting effects appear to be restricted to the lowest altitudes, where the kinetic energy densities associated with the noise floor removed KESD estimates (the solid line in Figure 2) are larger than the kinetic energy densities associated with the photon noise floors (the dashed line in Figure 2).

3.2. August 30, 1994

Measurements on August 30, 1994 commenced at 0326 UT (2326 LT) and ended at 0933 UT. The mean temporal KESD estimate over the altitude interval 31.6 - 37.8 km is shown in Figure 3 and has a slope of -1.60 ± 0.01 in the frequency range 4.62×10^{-5} s^{-1} to 1.00×10^{-3} s^{-1}. The high-frequency feature at 2.05×10^{-3} s^{-1} (1/(8.1 min)) is especially striking, rising an octave (or more) above its surroundings. Higher-frequency features at 4.10×10^{-3} s^{-1} (1/(4.0 min)) and 6.15×10^{-3} s^{-1} (1/(2.7 min)) are also apparent, although they are not as intense as the 2.05×10^{-3} s^{-1} feature. It should be emphasized that these high-frequency features are not an artifact of the processing routines used in this study as different averaging procedures, filters, "basic state" estimates, and spectral estimation techniques all reproduce these features at essentially the same power levels.

The intensity of these high-frequency features is very dependent upon the altitude range being considered. A contour plot of the high-frequency portion of the individual KE estimates that make up the mean KESD estimate is shown in Figure 4. The altitude dependence of these high-frequency features is quite apparent. The 2.05×10^{-3} s^{-1} feature has a maximum spectral density of 224 J s m^{-3} at 31.6 km and then decreases with altitude. The features at 4.10×10^{-3} s^{-1} and 6.15×10^{-3} s^{-1} exhibit a similar altitude dependence. It should be emphasized that this altitude dependence is not an artifact of the model order used in the PSD estimation process as correlogram and conservative, constant order autoregressive PSD estimates also reproduce this altitude dependence.

Although the altitude dependence of these high-frequency features is quite evident, Figure 4 provides little insight into the physical processes governing the growth rates obtained from these kinds of spectral estimates. Horizontal velocity spectral estimates, however, can provide a clearer insight into the physics of these features as linear wave theory allows one to compare the measured growth rates directly with the ρ^{-1} growth rates expected for linear gravity waves. Figure 5 shows the results of this comparison. All three of these features decay with height at rates that are significantly greater than ρ^{-1}, which suggests that the evolution of these features is being governed by some kind of nonlinear and/or dissipative process. However, this nonlinear and/or dissipative process is not able to dominate the evolution of these high-frequency features at all heights as occasional growth spurts with growth rates comparable to ρ^{-1} also appear in Figure 5 (e.g., the 33.0 - 34.0 km altitude region).

These high-frequency features also appear to be localized in time. To illustrate this, the relative density fluctuation field was

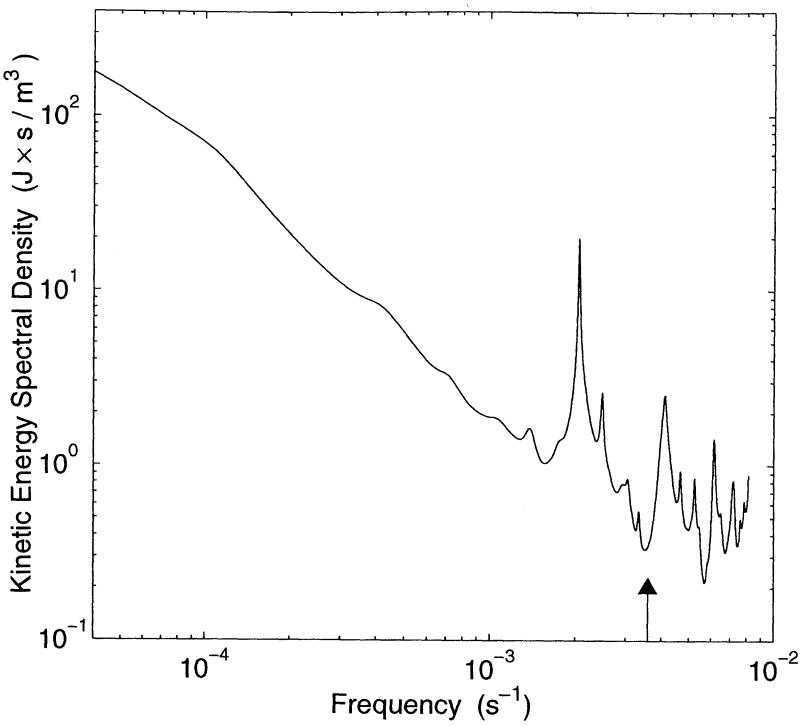

Figure 3. Temporal KE spectrum on the night of August 30, 1994, averaged over the altitude interval 31.6 km to 37.8 km. The photon noise floor has a mean value of 0.61 mJ s m^{-3} and has been removed from the spectrum. The arrow on the frequency axis indicates the average value of the measured buoyancy frequency for the altitude range under consideration (3.60 x 10^{-3} s^{-1}).

decomposed into six nonoverlapping 1 hour segments and detrended with a linear least squares fit. The resulting time series were then analyzed using the MUSIC algorithm [*Marple*, 1987] at a constant, conservative model order. Although the MUSIC algorithm is not a true PSD estimator in the sense that the area under the MUSIC "PSD" does not equal the power in the time series, it is very adept at finding sinusoidal features, especially in short time series [see *Sica and Russell*, 1999]. The resulting estimates are shown in Figure 6. The feature in the neighborhood of 3 x 10^{-4} s^{-1} to 4 x 10^{-4} s^{-1} is present over the entire measurement period. The feature at 2.05 x 10^{-3} s^{-1} is a bit more sporadic, being present during the second, third, fourth, fifth, and sixth hours of observation. The features at 4.10 x 10^{-3} s^{-1} and 6.15 x 10^{-3} s^{-1} are much more localized and only occur during the second and fourth hours of observation.

The presence of the higher-frequency features at 4.10 x 10^{-3} s^{-1}

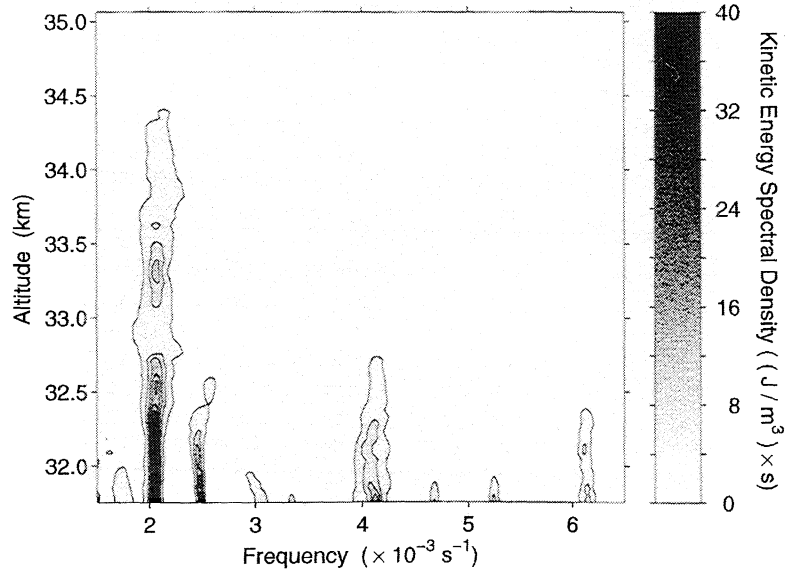

Figure 4. Individual KESD estimates on the night of August 30, 1994. The contour interval is 4.0 mJ s m^{-3} and has been chosen to highlight the altitude dependence of the high-frequency features.

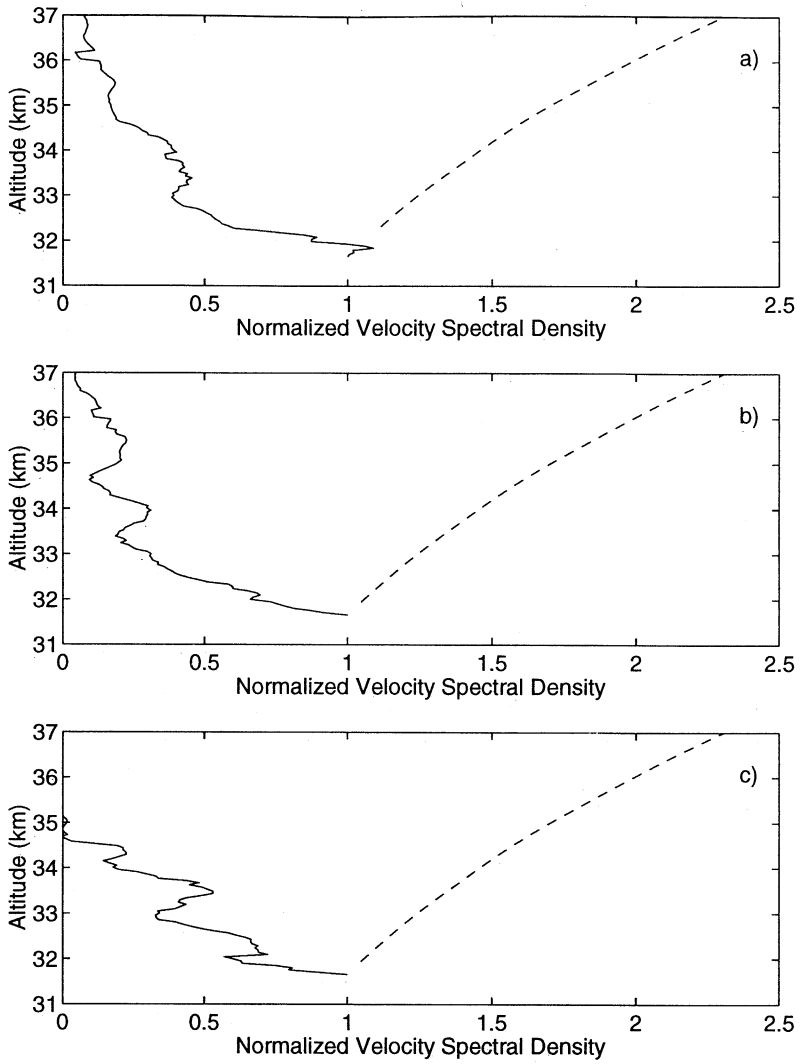

Figure 5. Normalized horizontal velocity spectral densities on the night of August 30, 1994 for (a) the 2 x 10^{-3} s^{-1} feature, (b) the 4 x 10^{-3} s^{-1} feature, and (c) the 6 x 10^{-3} s^{-1} feature. The dashed lines represent the ρ^{-1} growth rates predicted for "linear" gravity waves growing exponentially with height.

and 6.15 x 10^{-3} s^{-1} also suggests that substantial amounts of energy are being Doppler-shifted to frequencies higher than the measured buoyancy frequency (3.60 x 10^{-3} s^{-1}). These Doppler-shifting effects were again quantified by integrating the appropriate spectra from the measured buoyancy frequency to the Nyquist frequency. The kinetic energy densities associated with the noise floor removed KESD estimates (the solid line in Figure 7) are much larger than the kinetic energy densities associated with the photon noise floors (the dashed line in Figure 7) at the lowest altitudes, which suggests that significant amounts of energy are being Doppler-shifted to higher frequencies during these events.

3.3. October 13, 1995

Measurements on this night commenced at 0208 UT (2108 LT) and ended at 0916 UT. The mean temporal KESD estimate over the altitude interval 30.6 - 35.2 km is shown in Figure 8 and has a slope of -1.63 ± 0.01 in the frequency range 4.00 x 10^{-5} s^{-1} to 1.00 x 10^{-3} s^{-1}. Higher-frequency features at 2.09 x 10^{-3} s^{-1} (1/(8.0 min)) and 4.15 x 10^{-3} s^{-1} (1/(4.0 min)) are also apparent in this spectrum. As on the night of August 30, 1994, different averaging procedures, filters, basic state estimates, and spectral estimation techniques all reproduce these high-frequency features, which suggests that these high-frequency features are again real and not some artifact of the processing routines. These high-frequency features also appear to be dominated by some kind of nonlinear and/or dissipative process as these features also exhibit decay rates that are significantly greater than ρ^{-1}.

A MUSIC analysis of nonoverlapping 1 hour segments in the relative density fluctuation field suggests that the 2.09 x 10^{-3} s^{-1} and 4.15 x 10^{-3} s^{-1} features also exhibit some intermittency over the course of the measurement period (Figure 9) as the feature at 2.09 x 10^{-3} s^{-1} is present during the second, third, fourth, and seventh hours of observation, while the 4.15 x 10^{-3} s^{-1} feature is present during the third, fourth, fifth, sixth, and seventh hours of observation. The presence of these higher-frequency features also suggests that significant amounts of energy are being Doppler-shifted at the lowest altitudes (Figure 10). It should also be noted that the variance of the average temporal KESD estimate on

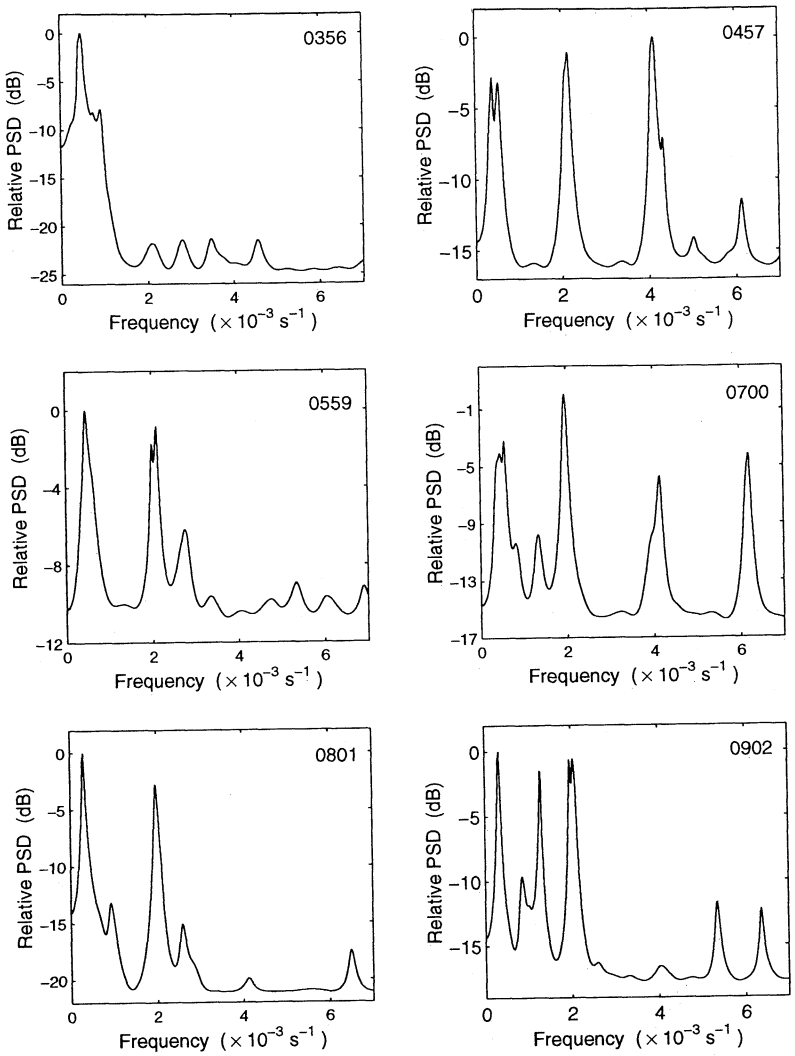

Figure 6. Mean 1 hour MUSIC power spectral densities (in dB) for the night of August 30, 1994. The time given in the upper right corner of each graph corresponds to the midpoint of the nonoverlapping time interval, for example, the first hour is in the upper left corner, the second hour is in the upper right corner, etc.

this night is greater than the variance of the average temporal KESD estimates in August, as would be expected from climatological considerations [*Hirota*, 1984; *Meek et al.*, 1985; *Hamilton*, 1991].

4. Discussion

The Doppler-shifting effects illustrated in Figures 2, 7, and 10 can also be seen in the spectral slopes of the mean KESD estimates. If the common "monotonic" range (e.g., 4.62 x 10^{-5} s^{-1} to 1.00 x 10^{-3} s^{-1}) of all three estimates is considered, it is evident from Tables 1, 2, and 3 that the spectral slopes at the lowest altitudes are much smaller than the expected values of -1.5 to -2.0. Spectral slopes in the higher-altitude regions, on the other hand, do fall within the expected -1.5 to -2.0 range. These facts suggest that significant amounts of energy are being Doppler-shifted at the lowest altitudes, in general agreement with the measured energy densities.

Despite the intermittency of the higher-frequency features on the night of August 30, 1994, there are two compelling facts about these features: The 4.10 x 10^{-3} s^{-1} and 6.15 x 10^{-3} s^{-1} features are always present at the same time and the 2.05 x 10^{-3} s^{-1} feature is always accompanied by a lower-frequency companion around 3 x 10^{-4} s^{-1} to 4 x 10^{-4} s^{-1}. One possible interpretation on the pairing of the 4.10 x 10^{-3} s^{-1} and 6.15 x 10^{-3} s^{-1} features is that they are an example of a nonlinear wave interaction. The parametric subharmonic instability (PSI) class of nonlinear triad interactions is particularly appealing in this regard as it models the decay of a small-wavenumber gravity wave into two large-wavenumber gravity waves of half the frequency [*McComas and Bretherton*, 1977; *Muller et al.*, 1986]. PSI growth rates are also known to be of the order of minutes [*Dunkerton*, 1989; *Sonmor and Klaassen*, 1997], which is well within the 1 hour time spans that these features are observed in. A more complete bispectral analysis of the density perturbation field obtained on this night would provide simultaneous information on the frequencies and vertical wavelengths of these features, which would then allow one to see if these features satisfy the appropriate PSI criteria. However, such a study is beyond the scope of this work and will have to wait until a two-dimensional spectral analysis toolbox has been developed and incorporated into the PCL processing routines.

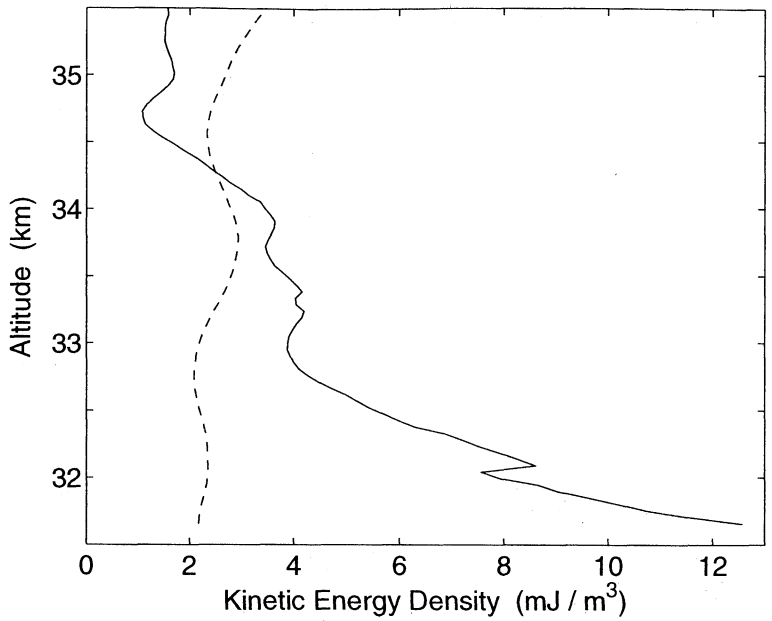

Figure 7. Estimated energy at frequencies greater than the buoyancy frequency on the night of August 30, 1994. The solid line represents the amount of energy past the buoyancy frequency in the KE spectra with the noise floor removed. The dashed line represents the amount of energy past the buoyancy frequency due to photon noise. The bump in KE energy at 32.3 km is due to a small irregularity in the model order selection process.

The presence of the 2.05×10^{-3} s^{-1} feature and a lower-frequency companion around 3×10^{-4} s^{-1} to 4×10^{-4} s^{-1} may be another example of an atmospheric instability. Such wave pairings have been observed by MU radar in the upper mesosphere [*Yamamoto et al.*, 1987] and have been attributed to a parametric instability or a convective instability. There is also another much more obvious but less intuitively satisfying interpretation to these high-frequency features: They are unrelated and just happen to occur at the harmonics of the first feature.

The high-frequency features on the night of October 13, 1995

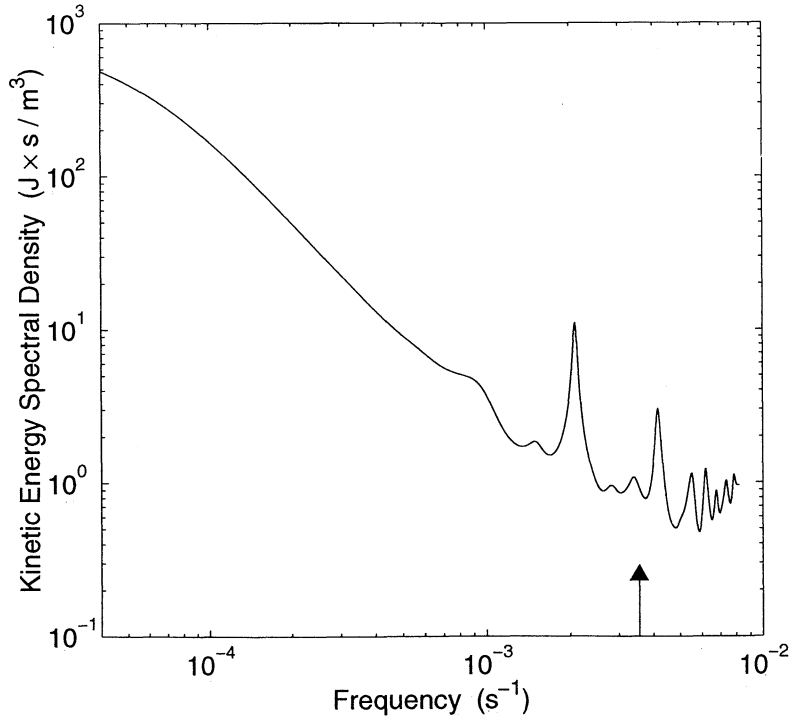

Figure 8. Temporal KE spectrum on the night of October 13, 1995, averaged over the altitude interval 30.6 - 35.2 km. The photon noise floor has a mean value of 0.85 mJ s m^{-3} and has been removed from the spectrum. The arrow on the frequency axis indicates the average value of the measured buoyancy frequency for altitude range under consideration (3.55×10^{-3} s^{-1}).

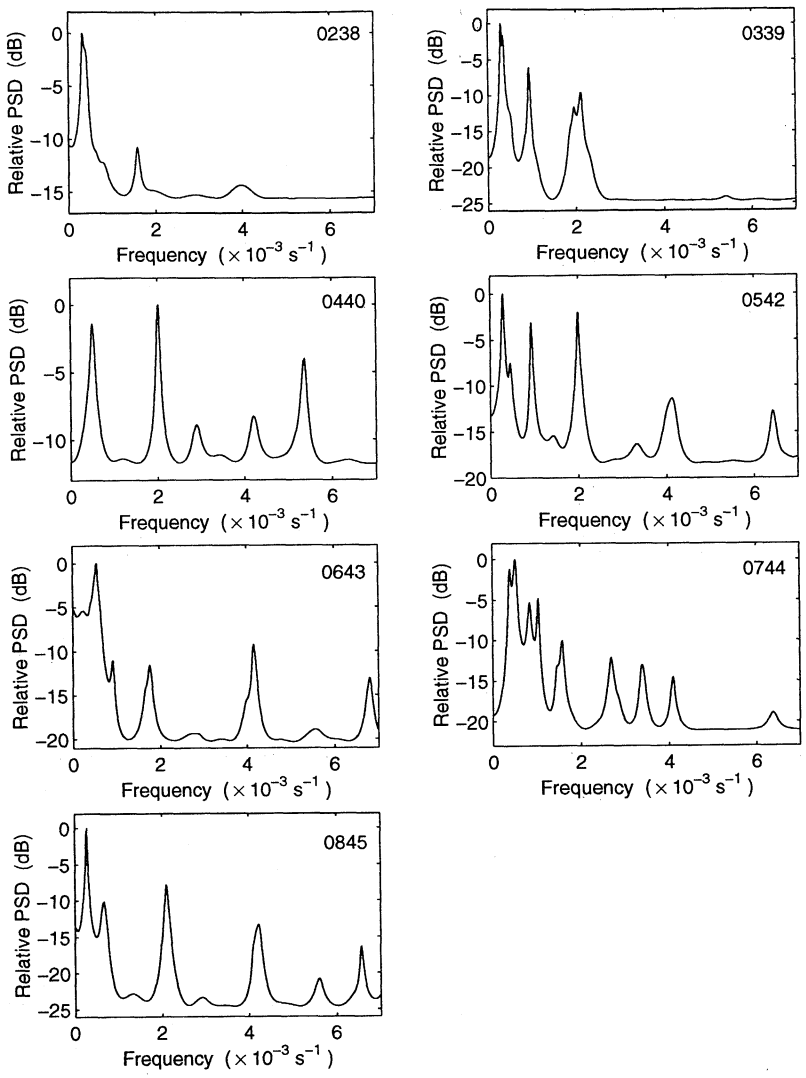

Figure 9. Mean 1 hour MUSIC "PSDs" (in dB) for the night of October 13, 1995. The time given in the upper right corner of each graph corresponds to the midpoint of the nonoverlapping time interval.

can also be interpreted in terms of instabilities; for example, the features at 2.09 x 10^{-3} s^{-1} and 3 x 10^{-4} s^{-1} to 4 x 10^{-4} s^{-1} may be an example of a parametric instability or a convective instability, while the features at 2.09 x 10^{-3} s^{-1} and 4.15 x 10^{-3} s^{-1} may be an example of a PSI. The possibility that these "wave pairings" are also coincidences cannot be discounted until a more complete bispectral analysis is performed.

Although the mechanism for generating these higher-frequency features cannot be confirmed at present, these spectra do exhibit larger total variances. Integration of the mean August 30 and October 13 KESD estimates over the appropriate frequency ranges has shown that these spectra have 2 to 3 times the power of the August 22 KESD estimate. This knowledge, when coupled with the intermittency and decay rates of these features, suggests that gravity wave activity in the middle upper stratosphere may often be larger and much more variable than assumed in the past.

These increases in gravity wave activity and variability can have dramatic effects on the dynamics of the middle upper stratosphere. Energy dissipation rates can be estimated from KESD estimates through the expression

$$\varepsilon = \int \omega KESD(\omega) d\omega = \int KESC(\omega) d\omega \qquad (2)$$

which suggests that energy dissipation rates in the middle upper stratosphere may also be larger and more variable than previously assumed. These increases in the amount and variability of energy dissipation also suggest that middle upper stratospheric eddy diffusion values may be larger and more variable than previously assumed. A more thorough discussion on estimating energy dissipation and eddy diffusion profiles (and the results obtained for August 30, 1994) was provided by *Sica* [1999].

A closer inspection of Figures 3 and 8 also suggests that there is an excess of energy before the measured buoyancy frequency. This excess of energy is not due to spectral leakage from the 2.0 x 10^{-3} s^{-1} feature as the covariance method of autoregressive PSD estimation is very adept at minimizing the effects of spectral leakage. One of the more obvious physical explanations for this excess is that the decreasing buoyancy frequency in the upper stratosphere is allowing higher-frequency gravity waves to interfere constructively, that is, as a packet of gravity waves propagates

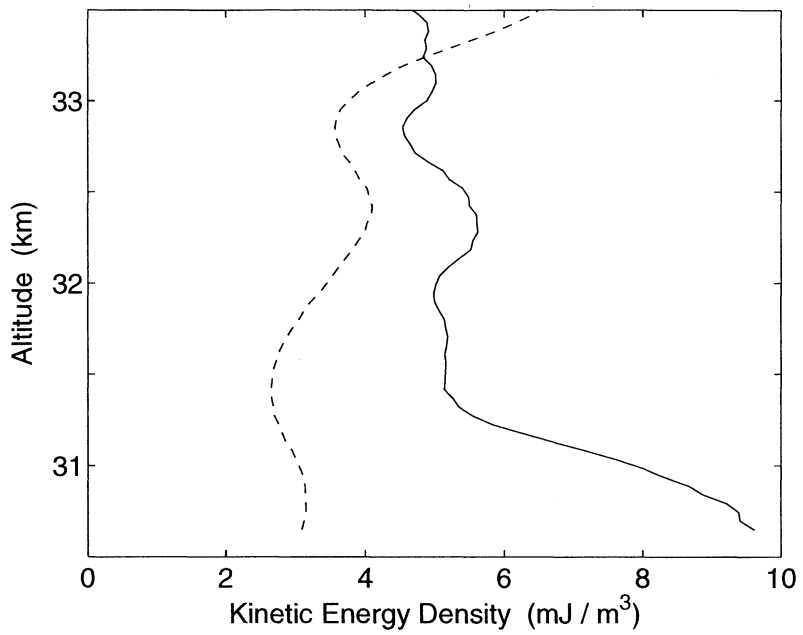

Figure 10. Estimated energy at frequencies greater than the buoyancy frequency on the night of October 13, 1995. The solid line represents the amount of energy past the buoyancy frequency in the KE spectra with the noise floor removed. The dashed line represents the amount of energy past the buoyancy frequency due to photon noise.

into the upper stratosphere, the decreasing buoyancy frequency causes gravity wave oscillations to become more vertical, which allows the higher-frequency gravity waves to interfere constructively as they are now more in phase with each other. However, this simple picture is complicated by the fact that the buoyancy frequency profile in the upper stratosphere is really a very dynamic quantity with many temporary small-scale superadiabatic layers being superimposed on the monotonically decreasing average [*Sica and Thorsley*, 1996, 1997]. It is also possible that this excess of energy might be due to the Doppler-shifting of shorter-period gravity waves. However, none of these suggestions can be confirmed until a more complete knowledge of the wind field and gravity wave propagation directions is obtained.

5. Conclusions

Middle upper stratospheric temporal KESD estimates obtained on three different nights have been presented. The frequency range of these estimates (1/(6 hours) to 1/(2 min)) is much larger than that of most previous studies in the middle upper stratosphere, extending the frequency range of current KESD estimates in this region to frequencies beyond the measured buoyancy cutoff. These KESD estimates exhibit the expected -1.5 to -2.0 power law relationship in the frequency range 4.6×10^{-5} s^{-1} to 1.0×10^{-3} s^{-1} and the expected seasonal magnitudes. Several high-frequency features were also present on the nights of August 30-31, 1994 and October 13-14, 1995 and have been attributed to nonlinear wave interactions. An excess of energy before the measured buoyancy frequency also exists, but the mechanism for generating this excess cannot be confirmed at the present time. It is also clear that the temporal KESD estimates are quite variable on shorter timescales and exhibit significant Doppler-shifting effects. These effects can have a significant impact on middle upper stratospheric dynamics and suggest that current parameterizations of subgrid dynamical processes in climate models of this region should be reevaluated. Recent high-resolution simulations by the SKYHI general circulation model also provide some support for this idea as the dynamical subgrid parameterizations currently being employed in SKYHI do not appear to represent the effects of unresolved scales at most altitudes correctly [*Koshyk and Hamilton*, 2000]. A more complete study on the seasonal characteristics of the temporal spectra in this region is planned for the future, which should allow more realistic middle upper stratospheric energy dissipation and eddy diffusion profiles to be constructed.

Table 1. Spectral Slopes on August 22, 1995

Altitude Range, km	Spectral Slope
34.9 - 35.9	-1.15 ± 0.02
36.0 - 37.0	-1.31 ± 0.02
37.0 - 38.0	-1.91 ± 0.01
38.1 -39.1	-2.03 ± 0.01
39.2 - 40.2	-1.62 ± 0.02
40.2 -41.2	-1.55 ± 0.03

Table 2. Spectral Slopes on October 13, 1995

Altitude Range, km	Spectral Slope
30.6 - 30.7	-1.46 ± 0.02
31.7 - 32.7	-1.53 ± 0.02
32.8 - 33.8	-1.85 ± 0.02
33.8 - 34.8	-1.87 ± 0.02

Table 3. Spectral Slopes on August 30, 1994

Altitude Range, km	Spectral Slope
31.7 - 32.7	-1.20 ± 0.03
32.7 - 33.7	-1.62 ± 0.02
33.8 - 34.8	-1.64 ± 0.02
34.8 - 35.8	-1.86 ± 0.02
35.9 - 36.9	-1.70 ± 0.02

Acknowledgments. We would like to thank G. P. Klaassen for many insightful discussions and comments, D. Kwarciak for his graphical wizardry, and the referees for their helpful comments. We would also like to thank and the National Science and Engineering Research Council, the Meteorological Society of Canada, and CRESTech for their financial support.

References

Allen, S. J., and R. A. Vincent, Gravity-wave activity in the lower atmosphere: Seasonal and latitudinal variations, *J. Geophys. Res., 100,* 1327-1350, 1995.

Bacmeister, J. D., S. D. Eckermann, P. A. Newman, L. Lait, K. R. Chan, M. Loewenstein, M. H. Profitt, and B. L. Gary, Stratospheric horizontal wavenumber spectra of winds, potential temperature, and atmospheric tracers observed by high-altitude aircraft, *J. Geophys. Res., 101,* 9441-9470, 1996.

Beatty, T. J., C. A. Hostetler, and C. S. Gardner, Lidar observations of gravity waves and their spectra near the mesopause and stratopause at Arecibo, *J. Atmos. Sci., 49,* 477-496, 1992.

Briscoe, M. G., Preliminary results from the tri-moored internal wave experiment IWEX, *J. Geophys. Res., 80,* 3872-3884, 1975.

Cairns, J. L., Internal wave measurements from a midwater float, *J. Geophys. Res., 80,* 299-306, 1975.

Collins, R. L., T. Xin, and C. S. Gardner, Gravity wave activity in the upper mesosphere over Urbana, Illinois: Lidar observations and analysis of gravity wave propagation models, *J. Atmos. Terr. Phys., 58,* 1905-1926, 1996.

Cot, C., and J. Barat, Wave-turbulence interaction in the stratosphere, *J. Geophys. Res., 91,* 2749-2756, 1986.

Desaubies, Y. J. F., A linear theory of internal wave spectra and coherences near the Vaisalla frequency, *J. Geophys. Res., 80,* 895-899, 1975.

Dunkerton, T. J., Theory of internal gravity wave saturation, *Pure Appl. Geophys., 130,* 373-397, 1989.

Ecklund, W. L., B. B. Balsley, D. A. Carter, A. C. Riddle, M. Crochet, and R. Garello, Observations of vertical motions in the troposphere and lower stratosphere using three closely spaced ST radars, *Radio Sci., 20,* 1196-1209, 1985.

Fritts, D. C., and T. E. VanZandt, Effects of Doppler shifting on the frequency spectra of atmospheric gravity waves, *J. Geophys. Res., 92,* 9723-9732, 1987.

Gardner, C. S., and D. G. Volez, Lidar studies of the nighttime sodium layer over Urbana, Illinois, 2, Gravity waves, *J. Geophys. Res., 92,* 4673-4694, 1987.

Gardner, C. S., M. S. Miller, and C. H. Liu, Rayleigh lidar observations of gravity wave activity in the upper stratosphere at Urbana, Illinois, *J. Atmos. Sci., 46,* 1838-1854, 1989a.

Gardner, C. S., D. C. Senft, T. J. Beatty, R. E. Bills, and C. A. Hostetler, Rayleigh and sodium lidar techniques for measuring middle atmosphere density, temperature, and wind perturbations and their spectra, in *World Ionosphere/Thermosphere Study Handbook,* vol. 2, edited by C. H. Liu, pp. 148-187, ICSU Sci. Comm. on Solar Terr. Phys., Urbana, Ill., 1989b.

Gardner, C. S., C. A. Hostetler, and S. A. Lintelman, Influence of the mean wind field on the separability of atmospheric perturbation spectra, *J. Geophys. Res., 98,* 8859-8872, 1993.

Gould, W. S., Spectral characteristics of some deep current records from the eastern North Atlantic, *Philos. Trans. R. Soc. London, Ser. A, 270,* 437-450, 1971.

Hamilton, K., Climatological statistics of stratospheric inertia-gravity waves deduced from historical rocketsonde wind and temperature data, *J. Geophys. Res., 96,* 20,831-20,839, 1991.

Hamilton, K., The role of parameterized drag in a troposphere-stratosphere-mesosphere general circulation model, in *Gravity Wave Processes: Their Parameterization in Global Climate Models,* edited by K. Hamilton, pp. 337-350, Springer-Verlag, New York, 1997.

Hirota, I., Climatology of gravity waves in the middle atmosphere, *J. Atmos. Terr. Phys., 46,* 767-773, 1984.

Koshyk, J. N., and K. Hamilton, The horizontal kinetic energy spectrum and spectral budget simulated by a high-resolution troposphere-stratosphere-mesosphere GCM, *J. Atmos. Sci.,* in press, 2000.

Manson, A. H., Gravity wave horizontal and vertical wavelengths: An update of measurements in the mesopause region, *J. Atmos. Sci., 47,* 2765-2773, 1990.

Marple, S. L., *Digital Spectral Analysis,* chap. 11, Prentice-Hall, Englewood Cliffs, N. J., 1987.

McComas, C. H., and F. P. Bretherton, Resonant interactions of oceanic internal gravity waves, *J. Geophys. Res., 82,* 1397-1412, 1977.

Meek, C. E., I. M. Reid, and A. H. Manson, Observations of mesospheric wind velocities, 2, Cross sections of power spectral density for 48-8 hrs, 8-1 hrs, and 1 hr to 10 min over 60-110 km for 1981, *Radio Sci., 20,* 1383-1402, 1985.

Moreels, G., and M. Hearse, Photographic evidence of wave around the 85 km level, *Planet. Space Sci., 25,* 265-273, 1977.

Muller, P., G. Holloway, F. Henyey, and N. Pomphrey, Nonlinear interactions among internal gravity waves, *Rev. Geophys., 24,* 493-536, 1986.

Rottger, J., Wind variability in the stratosphere deduced from spaced antenna VHF radar measurements, paper presented at 20th Conference on Radar Meteorology, Am. Meteorol. Soc., Boston, Nov. 30 to Dec. 3, 1981.

Scheffler, A. O., and C. H. Liu, The effects of Doppler shift on gravity wave spectra observed by MST radar, *J. Atmos. Terr. Phys., 48,* 1225-1231, 1986.

Sica, R. J., Measurements of the effects of gravity waves in the middle atmosphere using parametric models of density fluctuations, 2, Energy dissipation and eddy diffusion, *J. Atmos. Sci., 56,* 1330-1343, 1999.

Sica, R. J., and A. T. Russell, Measurements of the effects of gravity waves in the middle atmosphere using parametric models of density fluctuations, 1, Vertical wavenumber and temporal spectra, *J. Atmos. Sci., 56,* 1308-1329, 1999.

Sica, R. J., and M. D. Thorsley, Measurements of superadiabatic lapse rates in the middle atmosphere, *Geophys. Res. Lett., 23,* 2797-2800, 1996.

Sica, R. J., and M. D. Thorsley, Measurements of intermittency in the upper stratosphere and mesosphere, in *Gravity Wave Processes: Their Parameterization in Global Climate Models,* edited by K. Hamilton, pp. 27-44, Springer-Verlag, New York, 1997.

Sica, R. J., S. Sargoytchev, P. S. Argall, E. F. Borra, L. Girard, C. T. Sparrow, and S. Flatt, Lidar measurements taken with a large-aperture liquid mirror, 1, Rayleigh-scatter system, *Appl. Opt., 34,* 6925-6936, 1995.

Sonmor, L. J., and G. P. Klaassen, Towards a unified theory of gravity wave stability, *J. Atmos. Sci., 54,* 2655-2680, 1997.

Tolstoy, I., and H. Montes, Phase height fluctuations in the ionosphere between 130 and 250 km, *J. Atmos. Terr. Phys., 33,* 751-781, 1971.

Tsuda, T., Y. Murayama, T. Nakamura, R. A. Vincent, A. H. Manson, C. E. Meek, and R. L. Wilson, Variations of gravity wave characteristics with height, season, and latitude revealed by comparative observations, *J. Atmos. Terr. Phys., 56,* 555-568, 1994.

VanZandt, T. E., Gravity waves: Spectral decomposition of mesoscale fluctuations, in *Middle Atmosphere Program Handbook,* vol.16, edited by K. Labitze et al., pp. 149-156, SCOSTEP Secretariat, Univ. of Ill., Urbana, 1985.

Vincent, R. A., and D. C. Fritts, A climatology of gravity wave motions in the mesopause region at Adelaide, Australia, *J. Atmos. Sci., 44,* 748-760, 1987.

Voorhis, A. D., Measurements of vertical motion and the partition of energy in the New England slope water, *Deep Sea Res., 15,* 599-608, 1968.

Whiteway, J. A., and A. I. Carswell, Lidar observations of gravity wave activity in the upper stratosphere over Toronto, *J. Geophys. Res., 100,* 14,113-14,124, 1995.

Yamamoto, M., T. Tsuda, S. Kato, T. Sato, and S. Fukao, A saturated inertia gravity wave in the mesosphere observed by the middle and upper atmosphere radar, *J. Geophys. Res., 92,* 11,993-11,999, 1987.

A. T. Russell and R. J. Sica, Department of Physics and Astronomy, The University of Western Ontario, London, Ontario, Canada N6A 3K7. (sica@uwo.ca)

(Received April 18, 2000; revised September 21, 2000; accepted September 25, 2000.)